JOURNAL OF CHEMICAL INFORMATION AND MODELING

Article

pubs.acs.org/jcim

Molecular Dynamics Simulations of the Adenosine A2a Receptor: Structural Stability, Sampling, and Convergence

Hui Wen Ng,[†] Charles A. Laughton,[‡] and Stephen W. Doughty*,[†]

[†]School of Pharmacy, University of Nottingham Malaysia Campus, Jalan Broga, 43500 Semenyih, Selangor, Malaysia

[‡]School of Pharmacy, University of Nottingham, Nottingham, NG7 2RD, U.K.

Supporting Information

ABSTRACT: Molecular dynamics (MD) simulations of membrane-embedded G-protein coupled receptors (GPCRs) have rapidly gained popularity among the molecular simulation community in recent years, a trend which has an obvious link to the tremendous pharmaceutical importance of this group of receptors and the increasing availability of crystal structures. In view of the widespread use of this technique, it is of fundamental importance to ensure the reliability and robustness of the methodologies so they yield valid results and enable sufficiently accurate predictions to be made. In this work, 200 ns simulations of the A2a adenosine receptor (A2a AR) have been produced and evaluated in the light of these requirements. The conformational dynamics of the target protein, as obtained from replicate simulations in both the presence and absence of an inverse agonist ligand (ZM241385), have been investigated and compared using principal component analysis (PCA). Results show that, on this time scale, convergence of the replicates is not readily evident and dependent on the types of the protein motions considered. Thus rates of inter- as opposed to intrahelical relaxation and sampling can be different. When studied individually, we find that helices III and IV have noticeably greater stability than helices I, II, V, VI, and VII in the apo form. The addition of the inverse agonist ligand greatly improves the stability of all helices.

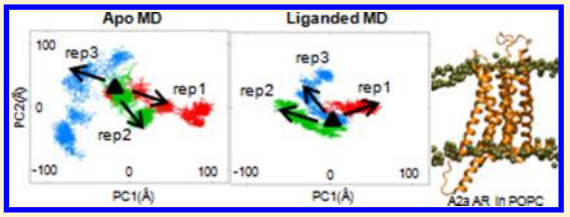

INTRODUCTION

The G-protein coupled receptors (GPCRs) are a versatile group of receptors due to their ability to respond to a vast array of neurotransmitters, hormones, and metabolites and trigger a complex cascade of cellular signaling processes. In addition, these receptors are also important targets for numerous biological products and small molecule drugs that have therapeutic values in a diverse range of diseases.[1−5] Close to half of all currently marketed drugs are GPCR-targeting;[6,7] approximately 24% of the new drugs that reached the market between 2000 and 2009 are GPCR ligands;[3] yet only an estimated 10% of all GPCRs are currently targeted.[8]

The adenosine A2a receptor (A2a AR) belongs to the family of adenosine receptors that also includes the adenosine A1, A2b, and A3 subtypes. These receptors are widely distributed and have therapeutic potential in some of the major disease areas involving the central nervous, respiratory, endocrine, inflammatory, renal, and cardiovascular systems.[9] For instance, ligands that target these receptors have been developed to treat Parkinson's disease (A2a AR antagonists),[10−12] diabetes (A1AR agonists),[13] and arthritis (A3AR agonists).[14]

Technological breakthroughs in recent years have seen the emergence of an increasing number of new GPCR crystal structures. To date, the GPCRs whose structures have successfully been elucidated are bovine rhodopsin (2000),[15] human β2 adrenergic receptor (2007),[16] turkey β1 adrenergic receptor (2008),[17] human A2a adenosine receptor (2008),[18] human CXCR4 chemokine (2010),[19] human dopamine D3 receptor (2010),[20] human histamine H1 receptor (2011),[21] human M2 muscarinic acetylcholine receptor (2012),[22] rat M3 muscarinic acetylcholine receptor (2012),[23] human sphingosine 1-phosphate (S1P1) receptor (2012),[24] mouse μ-opioid receptor (2012),[25] human κ-opioid receptor (2012),[26] mouse δ-opioid receptor (2012),[27] human nociceptin/orphanin FQ receptor (2012),[28] human CXCR1 chemokine receptor (2012),[29] NSRT1 neurotensin receptor (2012),[30] and PAR1 human protease-activated receptor (2012).[31]

The availability of GPCR crystal structures has not only led to a greater understanding of these important proteins but also propelled in silico studies of GPCRs to a new height. MD simulations have been performed on numerous GPCRs for various purposes over the years. Among these, studies have been carried out to investigate the molecular properties of GPCRs,[32−34] improve the understanding of GPCR−ligand binding and the associated ligand-induced structural changes on the protein[35−37] as well as to provide clues to the receptor activation process.[38,39] In addition, in the structure-based design of GPCR ligands, MD has been used to generate conformational ensembles which are used in virtual screening and docking studies.[40−43]

The robustness and reliability of MD simulations performed on GPCRs are of critical importance due to the widespread use of this technique. Users need to be assured of the reproducibility of the results and the relevance of the data generated before any meaningful conclusions can be drawn. In

Received: December 19, 2012
Published: March 21, 2013

dx.doi.org/10.1021/ci300610w | J. Chem. Inf. Model. 2013, 53, 1168−1178

this study, we have sought to apply robust, sensitive, and quantitative metrics to investigate this and also to attempt to answer some of the common technical questions that may arise while performing these simulations: How good are my models/systems? How long should the equilibration process be? Are my results sufficiently reliable and reproducible such that meaningful observations can be made and conclusions drawn? A detailed understanding of the inherent limitations of the technique and the errors that may arise will help the users to be judicious in interpreting their results.

For this study, 200 ns simulations of the A2a adenosine receptor (A2a AR) in its apo form as well as in complex with an inverse agonist ligand (ZM241385) were carried out. The simulations were performed in triplicate, replicates differing only in their initially assigned velocity distributions. Using principal component analysis (PCA), we have systematically compared the replicate simulations and assessed the convergence and reproducibility of the results. PCA was used to study the molecular motions of the A2a AR at different levels: (1) the whole protein, (2) the transmembrane (TM) regions, (3) within helices I−VII individually, and (4) between the TM helices (i.e., looking at the interhelical dynamics of the TM region after removing all intrahelical motions). PCA is an ideal tool to study molecular behavior because of its ability to reduce the dimensionality of complex molecular motions to a small number of large-scale, often functionally important modes. It is also a powerful tool that provides quantitative metrics to test whether two different simulations are exploring the same conformational space and the level of sampling that occurs in a simulation.

PCA has been used in a number of studies to investigate the molecular motions of proteins[44−49] including GPCRs.[50−52] The issues of sampling time length, simulation convergence, and the difficulties in assessing and achieving a fully converged sampling have been recurrent themes in these works. In the earlier studies, time scales ranging from subnanoseconds to 10 ns have highlighted the problem of insufficient simulation time. The difficulties in identifying reliable modes have become apparent in these studies.[46,48] While Amadei et al. have concluded that the determination of essential and near constant subspaces could be achieved in simulations of a few hundred picoseconds,[47] later studies with up to the hundred nanosecond time scale have shown that convergence and undersampling are still a problem.[49−51] In a recent study, Romo et al.[53] have conducted microsecond scale simulations on proteins of varying sizes and measured the extent of convergence with different methods. Their findings have reemphasized the difficulties of achieving convergence and adequate sampling in proteins especially when the protein size increases. The GPCRs that have been studied with PCA so far are rhodopsin, the β2 adrenergic receptor, and CB2 cannabinoid receptors.[50−52] These studies have explored and analyzed the dynamics of different parts of the protein (whole protein, TM, and loop regions). This study adds the ARs to the list of GPCRs whose dynamics have been investigated with the PCA method. However, what really sets this study apart from the rest is that, on top of the whole protein and TM dynamics analyses, the molecular motions of GPCR helices have also been explored and described individually in detail. This presents a good opportunity to delve further into the core of GPCR dynamics and uncover the intrinsic behavior of these helices—the crucial building blocks of the all-important TM region of the GPCRs. Our findings, besides leading us to revisit the age-old problem of sampling and convergence in MD, have also revealed interesting dynamic behaviors associated with the helices which change upon ligand binding.

METHODS

Model Construction. The crystal structure of engineered A2a AR at 2.6 Å resolution (3EML)[18] was obtained from the Protein Data Bank. The 160 residue long T4-lysozyme portion (N1002−N1161), SO^{4-} ions, and stearic acid molecules were deleted. The ligand ZM241385 was (i) left in place for the liganded model and (ii) removed to create the apo form. Crystallographic waters were preserved. The missing residues in the crystal structure were added using the *loop search* tool in SYBYL 6.5.[54] These were M1-I3 (N-terminus), P149−H155 (extracellular loop 2, EL2), and K209−A221 (intracellular loop 3, IL3). The final structures lacked the C terminus and contained only residues 1−310. A brief round of steepest descent energy minimization was performed using the GROMOS96 53A6 force field[55] in GROMACS 4.5.3[56−58] to remove any steric clashes in the models arising from the loop building. The quality and integrity of the final A2a AR models were checked using PROCHECK[59] and WHATIF.[60] For both models, the validation programs did not report any critical problems and more than 99% of the residues were found in the allowed region of the Ramachandran plot. Therefore, they were considered fit for production simulations.

ZM241385 Parameterization. PRODRG beta[61] was used to generate the topology of ZM241385 and to assign atom types and bonded parameters. To deal with the potential lack of accuracy of PRODRG generated charges and charge groups, these values were reassigned following the strategy suggested by Lemkul et al.[62] This task was achieved by deriving charges and charge groups from known functional groups found in the amino acid residues topologies defined in the GROMOS 53A6 force field. (The topology can be found in Supporting Information Figure 1.)

System Setup and Simulation Protocols. The energy minimized A2a AR models (apo and liganded) were inserted into a pre-equilibrated and fully hydrated POPC lipid bilayer of 340 molecules. The bilayer was constructed and tailored to the intended size using the original "Berger lipids"[63] (obtained from http://moose.bio.ucalgary.ca/). The embedding process was achieved using the *g_membed* tool[64] which was available as part of GROMACS 4.5.3. The water model used was the single point charge (SPC)[65] model. To remove the net charge of the system, 11 chloride ions were added as counterions. The equilibration process started with a 100 ps simulation under *NVT* conditions at 310 K. The simulation parameters were as follows: electrostatic interactions were treated with the smooth particle mesh Ewald (PME)[66] method with a short-range cutoff of 1.2 nm, van der Waals interactions were also given a short-range cutoff of 1.2 nm, all bonds were constrained with LINCS[67] to enable a 2 fs time step to be applied, and temperature was coupled to the v-rescale[68] thermostat with a time constant of 0.1 ps. Coordinates were written to the output trajectory file every 100 ps. Position restraints were applied to the heavy atoms of the A2a AR model along the x, y, and z axes as well as the phosphorus atom of POPC along the z axis only, where $x-y$ is the membrane plane. Under these restraints, the water molecules were allowed to move in all directions while the lipids were able to do so only in the $x-y$ plane. After *NVT*, three separate rounds of *NPT* were carried out to allow the position restraints to be gradually released. Maintaining the

dx.doi.org/10.1021/ci300610w | J. Chem. Inf. Model. 2013, 53, 1168−1178

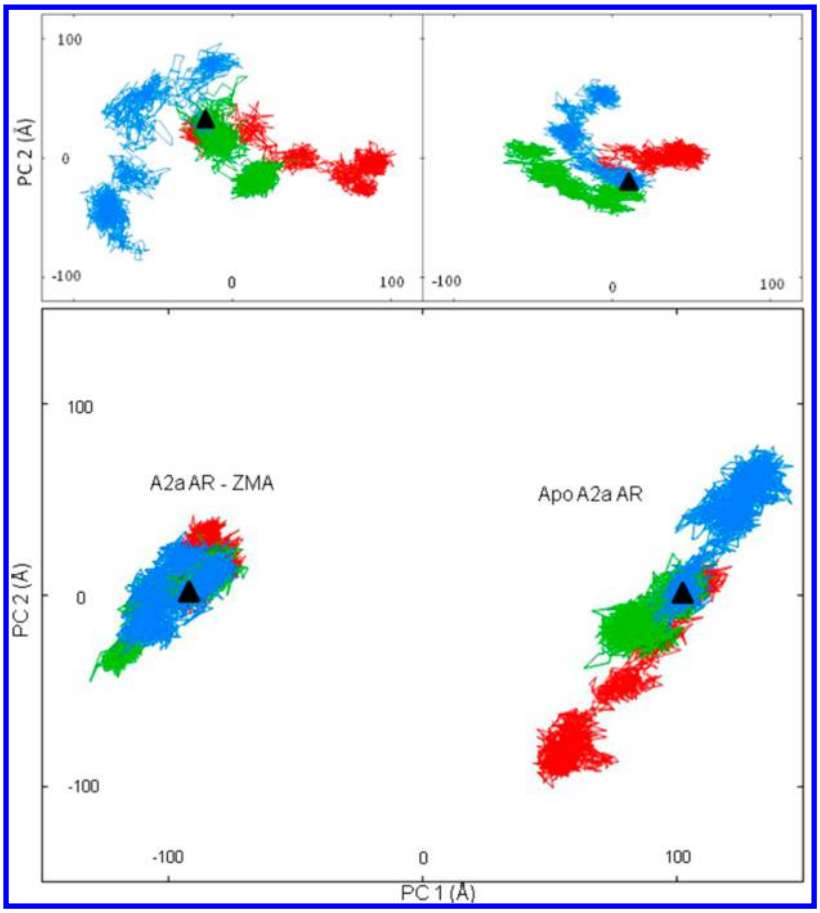

Figure 1. Projections of the apo A2a AR and A2a AR-ZMA simulations onto the common subspaces defined by the PC1/PC2 for the whole protein when (top left and top right) the two systems are analyzed independently and (bottom) together: (red) replicate 1, (green) replicate 2, (blue) replicate 3, (▲) conformation at the start of the production phase.

restraints from the *NVT* stage, the first round of *NPT* was carried out for 10 ns, with semi-isotropic pressure coupling to the Parinello-Rahman barostat[69] and a time constant of 1 ps. The second round was performed for 20 ns with position restraints applied only to the protein. All the position restraints were removed in the third round, and the systems were allowed to equilibrate for 40 ns. Finally, production simulations of 200 ns were performed in triplicate under the same NPT conditions. The only difference between replicates was in the initial velocity assignments at the start of the dynamics. Typically, ca. 20 ns of simulations could be achieved per day using ten Quad-Core 3.00 GHz Harpertown CPUs and 8 Gb of RAM.

Analysis. Principal component analysis was performed using our in-house toolkit *pcazip* (http://holmes.cancres.nottingham.ac.uk/pcazip). The GROMACS generated trajectories which contained 2000 snapshots (coordinates were saved every 100 ps) of the system were compressed and processed using these tools. In all cases, the data for the three replicates for each of the apo and ligand-bound systems was combined before PCA, so the dynamics of replicates could be compared within a common subspace. Focusing on the backbone of the protein, the analysis was divided into four parts. First, the protein was considered as a whole. This was followed by the analysis just of the TM region (i.e., excluding all loop residues). Next the pure interhelical motions of the TM region were studied. To achieve this, for each snapshot in each trajectory, copies of each individual helix, in the crystal structure conformation, were least-squares fitted to the respective sections of the snapshot structure and used to generate a pseudotrajectory in which the seven helices appear to move relative to each other as rigid bodies. This was then used for the PC analysis. Finally helices I–VII were analyzed individually (see Supporting Information Table 1 for residues found in each helix). To visualize the major relaxation processes, we looked at the trajectories when projected onto the two-dimensional subspace defined by the top two principal components (PC1 and PC2). In this study, PC1 and PC2 alone typically account for about half of the overall motions (importance of the remaining PCs decrease dramatically thereafter). Therefore they are deemed an adequate, albeit rough, representation of the overall dynamics of the system. However, PC3 was also taken into account to generate additional PC1/PC3 and PC3/PC2 projections to further verify the results of the intrahelical motions obtained (see the Results section for rationale). For the top n PCs that capture 90% of the variance, the dot products and subspace overlaps between the replicate simulations were also calculated using *pcazip*. The backbone root-mean-square fluctuations (RMSF) and root-mean-square deviations (RMSD) were calculated using GROMACS 4.5.3. The PCA, RMSF, and RMSD plots were generated using gnuplot.[70] The residues interacting with ZM241385 in the 3EML crystal structure were identified using Ligplot[71] together with visual inspection. The porcupine plots were generated using a perl script[72] and VMD.[73] The PC1/PC3 plots, PC3/

dx.doi.org/10.1021/ci300610w | J. Chem. Inf. Model. 2013, 53, 1168–1178

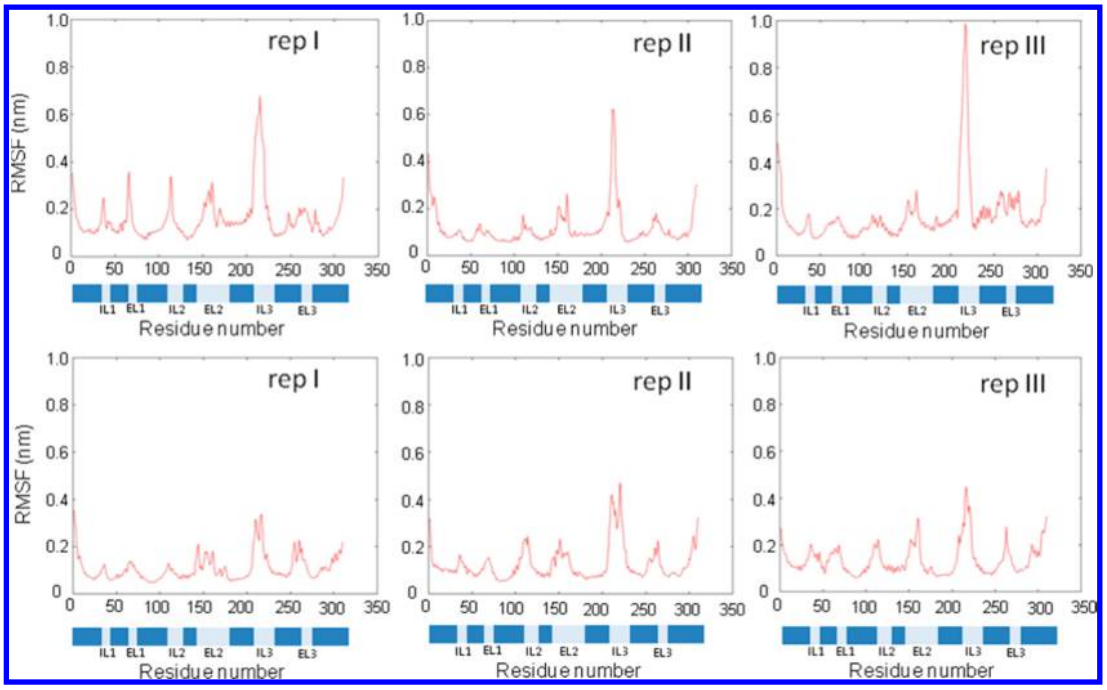

Figure 2. RMSF for residues 1−310 of apo A2a AR (top) and A2a AR-ZMA (bottom).

PC2 plots, RMSD, and porcupine plots are presented in the Supporting Information.

RESULTS

Overall Protein Behavior: Apo A2a AR and A2a AR-ZMA Systems. The projections of the apo A2a AR and A2a AR-ZMA trajectories onto the common subspace defined by the top two PCs are shown in Figure 1 in two ways: (1) when the two systems are considered separately (top) and (2) when both systems are considered together (bottom).

In 1, three things are immediately obvious from these projections. First, all simulations show a more or less continuous drift away from the conformation at the start of the production phase. Second, replicate simulations drift away along distinct paths. Third, the simulations of the apo protein are more divergent than those of the ligand-bound form.

From 2, we see that if we attempt to use a common subspace to analyze both apo and ligand-bound simulation systems, the analysis is dominated by the structural adjustment that accompanies ligand binding. This is clearly of greater magnitude than any structural perturbation that goes on during an individual MD simulation. Since it is perfectly reasonable that ligand binding has this effect, but that for our purposes here this structural variation is not of direct interest and "swamps" the more subtle conformational adjustments observed within and between replicates of each system, for the rest of the analyses we always perform the PCA analysis on the two systems independently.

Animations of the structures along the principal components reveal that they represent complex collective motions (results not shown). However it is clear that much of the dynamics is concentrated in the extra- and intracellular loop regions, as might be expected. This is evident from the calculation of root-mean-square fluctuations of each amino acid (Figure 2). We see that IL3 is the most dynamic feature in all replicate simulations and that, in agreement with the PC subspace plots in Figure 1, overall dynamics is somewhat suppressed by ligand binding. Interestingly, the crystal structure reveals no direct contact between ZM241385 and IL3 (Figure 3); extracellular loops 2

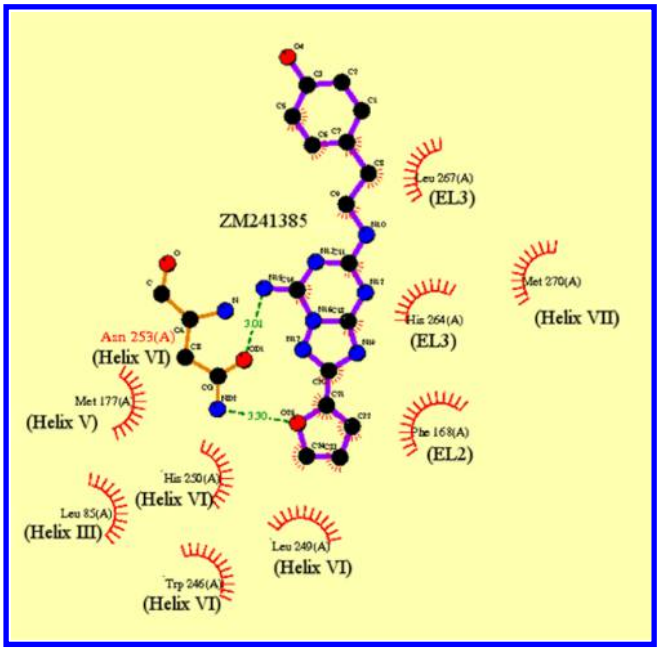

Figure 3. Ligplot of 3EML crystal structure showing the ZM241385 inverse agonist and the surrounding interacting residues.

and 3 are much more involved, yet the effect of ligand binding on their dynamics is much more subtle. The fact that the rigidification of IL3 on ligand binding is a consistent feature in all replicates of the simulation increases our confidence in its authenticity; however, at present the mechanism by which the allostery comes about is unclear. We must also bear in mind that since the evidence here is that the simulations are not well converged, the biological significance of this observation cannot be assured.

dx.doi.org/10.1021/ci300610w | J. Chem. Inf. Model. 2013, 53, 1168−1178

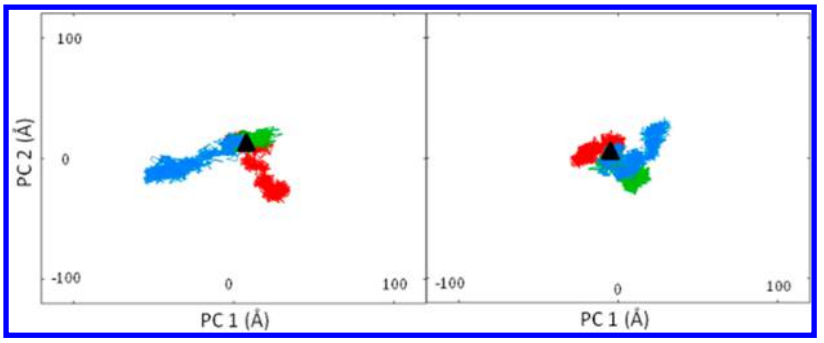

Figure 4. Projection of the apo A2a AR (left) and A2a AR-ZMA (right) simulations onto the common subspaces defined by the PC1/PC2 for the TM backbone region.

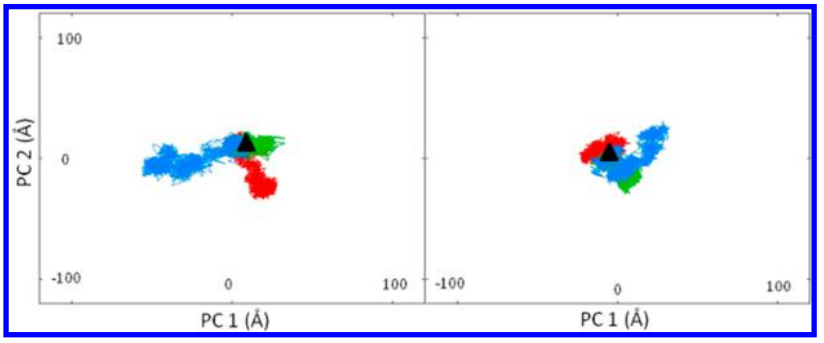

Figure 5. Projection of the apo A2a AR (left) and A2a AR-ZMA (right) simulations onto the common subspaces defined by the PC1/PC2 for the interhelical motions of the TM backbone. These plots are almost perfectly identical with Figure 4.

TM-Region Behavior: Apo A2a AR and A2a AR-ZMA Systems. The TM helical bundle is a portion of the protein that is most structured. Confined in a lipid environment, these helices have less freedom to move compared to the intra- and extracellular loops. However, we know from the crystal structure that they contribute to the majority of the binding site cavity and, so, may be expected to have dynamics that is sensitive to ligand binding.[15−18,74−79] Performing the PCA on the helical portions of the structure alone (Figure 4), we note a number of features. First it is clear by comparison with Figure 1 that the dynamics of this region is indeed reduced in comparison to the loops. However all observations made for the protein as a whole still hold true; the conformations of the helical region drift away from the conformation at the start of the production phase over the course of the MD simulations, the individual replicates drift away along (fairly) distinct paths, and the drift for the ligand-bound replicates is less marked than for the replicates of the apo protein.

Visualization of the motions corresponding to the principal components again reveals that they are capturing complex collective motions (result not shown). To simplify the interpretation of the dynamics of the system, we have therefore dissected this dynamics into inter- and intrahelical components.

Interhelical Behavior: Apo A2a AR and A2a AR-ZMA Systems. Figure 5 shows the projection of the simulations onto the common subspace defined by the PC1/PC2 plane for the interhelical motions of the TM backbone. It is interesting to note that, from a comparison with Figure 4, the pattern of motion is almost perfectly identical. Two points come across clearly from this: an exceedingly vast majority of the dynamics of the TM region may be regarded as rigid body motions of individual helices relative to each other; these interhelical motions do not resemble each other among the replicate simulations.

Visualization of of the most significant interhelical motions (PC1) has revealed generally larger and more varied movements in apo A2a AR than A2a AR-ZMA simulations. A range of different helical motions, e.g. sliding, rocking, bending, and twisting of the helices was observed. On the whole, the motions in the apo simulations led to the expansion and contraction of the binding pocket. For example, animations of PC1 of apo A2a AR replicate 3 shows that helices I, VI, and VII experience much larger movements particularly in the extracellular portion compared to helices II, III, IV, and V. The concerted movements of these helices (e.g., when helix VII moved away from the active site, helices I and VI moved toward it) had led to pronounced changes in the active site volume. On the other hand, the occupation of ZM241385 in the binding pocket had led to a significant dampening of the overall helical motions therefore resulting in smaller active site volume fluctuations (see Supporting Information Figure 2 for porcupine plots)

Intrahelical Behavior: Apo A2a AR and A2a AR-ZMA Systems. While it is clear from the above that interhelical dynamics dominates the conformational flexibility of this system, intrahelical motions cannot be neglected. In particular it seems clear that the degree of divergence observed in the dynamics of individual replicates could be manifested at the intrahelical level. Performing PCA on the TM helices individually, we see that this is indeed the case. We see that different helices show quite different degrees of flexibility and quite different degrees of dynamical reproducibility. For the apo simulations (Figure 6) the most rigid helix is helix IV. Helices I, III, and V are more dynamic but in a consistent way across the replicates. Helices II, VI, and VII are the most dynamic and the most variable in their behavior between replicate simulations.

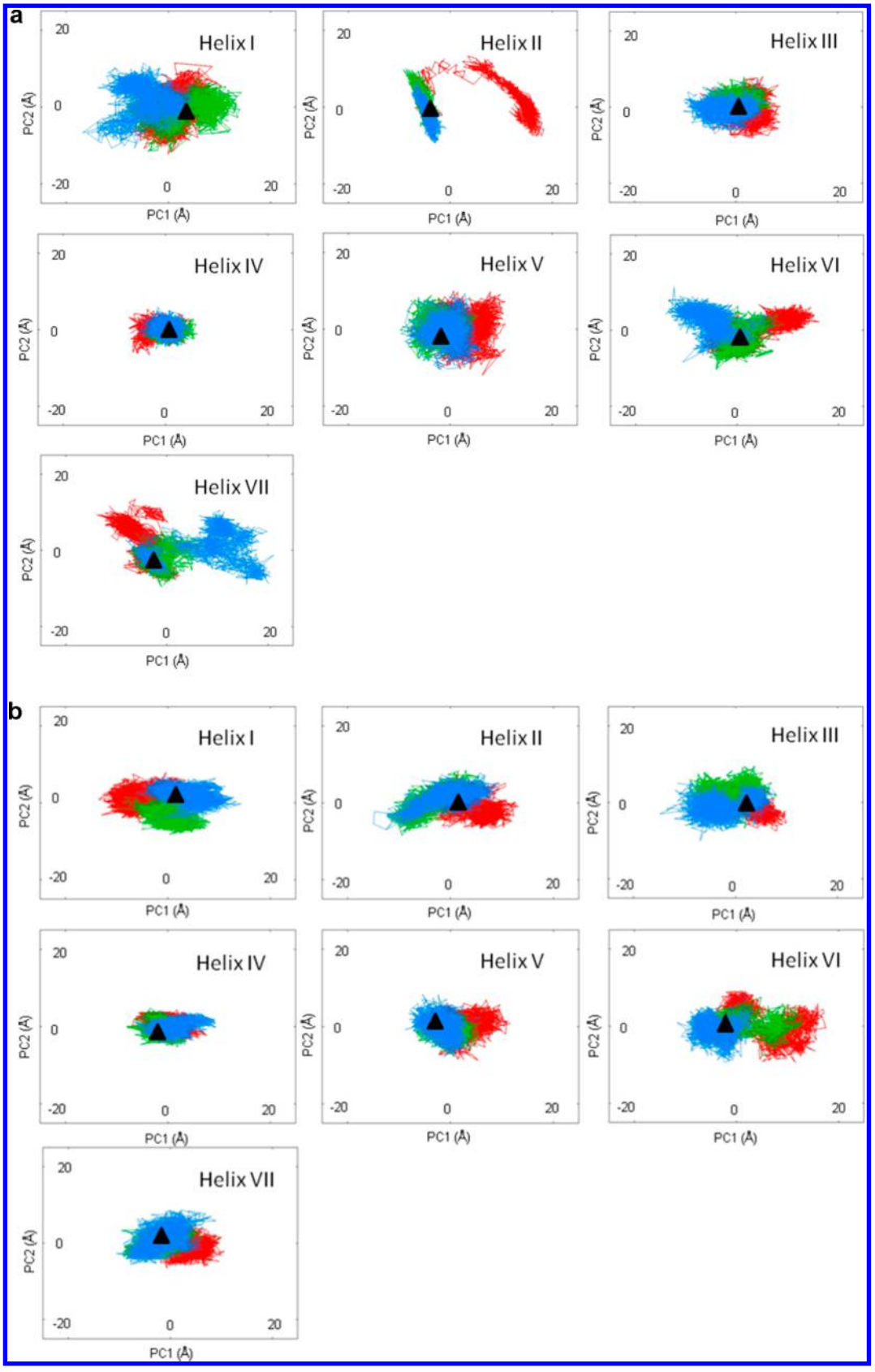

Figure 6. (a) Projection of the apo A2a AR simulations onto the common subspaces defined by the PC1/PC2 for the individual helices. (b) Projection of the A2a AR-ZMA simulations onto the common subspaces defined by the PC1/PC2 for the individual helices.

Looking now at the behavior of the helices in the presence of bound ligand (Figure 6b), we see that the result is a marked increase in the reproducibility of the dynamics in helix II, though it remains quite dynamic; that helix VII becomes

dx.doi.org/10.1021/ci300610w | J. Chem. Inf. Model. 2013, 53, 1168−1178

somewhat more rigid and somewhat more consistent in its motion, but that the behavior of helix VI is largely unchanged. It is interesting to note that few of these observations are easily predictable on the basis of the crystal structure data (Figure 3). Thus there are no direct interactions between helix II and ZM241385, yet its dynamic is clearly sensitive to the presence of the ligand. Conversely, there are direct interactions between the ligand and helix VI, yet it seems to remain insensitive to the occupation or otherwise of the binding site. The clear response of helix VII to ligand binding is however as one might expect from the interactions visible in the crystal structure.

Conscious of the pitfalls of viewing these results from only one perspective i.e. the two-dimensional PC1/PC2 subspace, additional plots of PC1/PC3 and PC3/PC2 have been generated (see Supporting Information Figures 3 and 4). These provide further verification that the overlaps observed between the replicates are indeed real and not an artifact of our analysis protocol. Apart from that, as a means to demonstrate and quantify the changes in the extent of replicate simulations overlap observed throughout the study, the dot products and subspace overlaps between the replicate simulations have also been calculated (see Supporting Information Figures 5–9). All in all, consistent with our findings, a clear increase in subspace overlap was observed from the overall protein (ca. 0.500–0.600) to the intrahelical (ca. 0.800 and above) analyses. A similar scenario was also found in the dot products whereby a rise in the conservation of the individual PCs between the simulations were noted as the study progressed.

DISCUSSION

One of the first lessons learned from the whole protein and TM region analyses is that the protein is still experiencing an ongoing relaxation process which takes place in a random and protracted manner throughout the 200 ns simulation. The finding leads to a number of conclusions: (1) the progression toward an equilibrated state for our target protein does not occur in a single prescribed route; (2) the protein drifts away from the conformation at the start of the production phase over the course of simulation; (3) the simulation time scale is not long enough to ensure convergence. It has also become apparent from this study that even by using the *g_membed* method for protein insertion, one that is believed to minimally perturb the properties and hydration of a pre-equilibrated lipid bilayer,[64] long equilibration time is still necessary for certain proteins to fully relax within a lipid environment. Our analysis of the simulations—particularly the divergent behavior of replicates—leads us to conclude that the problem is not so much with the system setup process as with the inherent slow dynamics and complex energy landscape. These conclusions would not have been nearly so apparent from other metrics commonly used to measure the convergence of simulations such as the RMSD (see Supporting Information Figure 10 for the RMSDs calculated for these simulations).

The issue of convergence in computational simulations has long been a topic of interest. Lyman et al.[80] have described a converged system as one that has sampled all possible states at the correct intervals and probabilities according to Boltzmann factor. They have also pointed out the challenges of assessing the quality of a simulation and determining true convergence due to inherent statistical errors.[80] At the outset, true convergence is enormously difficult to achieve. In fact instead of absolute convergence, the concept of relative convergence has been raised previously by other groups.[80,81] We are in agreement with Grossfield and co-workers[51] that a simulation is considered valid and sufficiently converged if it is performed long enough for a reliable prediction to be made in order to answer a specific question. However, an excellent example demonstrated in another piece of work also by Grossfield et al.[81] had shown that even this was not straightforward: the 50, 150, and 1600 ns simulations of dark state rhodopsin gave significantly different conclusions when analyses were performed on the torsion of the ionone ring (found as part of the covalently bound retinal ligand). In that study, the torsional state of retinal which was considered as a local degree of freedom was expected to relax in a reasonably short time. The 1600 ns simulation had revealed an increase in the trans state population as a result of the slow relaxation of the internal degrees of freedom of the whole protein. This outcome was unforeseen in the two shorter durations and aptly highlighted the risk of not performing a long enough simulation.[81]

Our results have shown an increase in the degree of convergence of the simulations after the elimination of the loop regions from the analyses. This points toward the fact that the loop regions were the most under-sampled—an observation which is consistent with the findings from other groups.[50,51] The RMSF analysis has also revealed an interesting observation whereby the mobility of the IL3 was most affected by ligand binding compared to the other loops despite the fact that it had no direct contact with the ligand. While the reason for this is unclear to us, the role of IL3 in ligand-induced coupling to the G-proteins is, however, a well-known fact.[82−84]

A higher degree of convergence is expected in the TM region analyses (particularly in the bound form) because this region is more well-structured compared to the rest of the protein. However, dissimilarities between the replicates are still obvious in both the bound and unbound form although more pronounced in the latter. We have found that this was largely attributed to the differences in the interhelical motions. This finding coincides with the observations made by Deupi et al.[85] in their study of β2 adrenergic receptor using atomic force microscopy whereby their results showed that the binding of ligands (agonists, antagonists, and inverse agonists) has little effects in stabilizing interhelical interactions. They had also suggested that an inverse agonist (carazolol in Deupi's case) promotes the receptor to sample a different conformational space that prevents the receptor from being activated, much as an agonist promotes the opposite.[85]

The PCA of the intrahelical motions have shown a large increase in convergence. Comparing the bound and unbound forms, the latter had shown more random behaviors than the former. This is in accord with the currently held view that, in the unbound form, the GPCRs sample a wide conformational space and exist in multiple states (e.g., inactive R, activated R*, etc.). The binding of a ligand shifts this equilibrium toward a specific state; in this case, the inactive state considering the inverse agonistic role of ZM241385. We have managed to associate distinctive dynamical behaviors with the individual helices. Helix IV is predicted to be the most stable helix, demonstrating the least movement with regards to the inter- and intrahelical motions and in both apo and ligand-bound systems. This helix has not been found to interact with any of the agonists, antagonists, and inverse agonists currently cocrystallized with A2a AR.[18,78,79,86−89] When in the unbound form, we found that helices I, III, and V were more dynamic in a consistent manner while helices II, VI, and VII were more dynamic in a variable way. These dynamics are slightly different

from those reported by Deupi et al.[85] on the apo form of β2 adrenergic receptor whereby helices III, IV, and V were found to have a relatively high flexibility. While Deupi et al.[85] reported that the binding of carazolol to β2 adrenergic receptor led to increased conformational changes in helices I, III, IV,V,VI,VII, and VIII, the binding of ZM241385 has caused the variation of the helices between the replicate simulations to reduce significantly with the exception of helix VI.

Experimentally, the rearrangement of the individual helices in the 7-TM bundle has been found to be central to the activation process; the movement of helices III, V, VI, and VII have been reported to play an important part in A2a AR activation.[78,79] Helices V−VII have been reported to experience larger movements during the activation process compared to helices I−IV which were described as the more stable helical bundle "core".[78] The dramatic movement of helix VI in receptor activation[74,79] has made it particularly noteworthy: This helix contains part of the "ionic lock" (E6.30 with R3.50 of the E/DRY motif) that seems to stabilize receptors in an inactive conformation and is where the "toggle switch" (W6.48) resides.[90,91] Apart from that, it also contains a kink at the conserved P6.50 which is believed to be involved in maintaining receptors at an inactivate state.[92] Although our results do not cover the dynamics of an agonists bound A2a AR, they have shown a considerable degree of flexibility in helix VI in both the absence and presence of a ligand, which highlights its propensity to remain highly mobile. Visualization of trajectories shows that, in our apo A2a AR simulations, the P6.50 kink "straightened" significantly while W6.48 was perceived to fluctuate between the states where it was parallel (toward active state) and perpendicular (starting/toward inactive state) to the membrane plane.[93] While the starting structure contained a broken "ionic lock", it was found that two residues of this lock had moved closer to each other causing the lock to be repeatedly reformed and broken during the course of the simulations. On the other hand, for the A2a AR-ZMA simulations, the P6.50 kink as well as W6.48 were found to remain relatively unchanged from the starting states. The two residues of the "ionic lock" were again found to be constantly formed and broken during the simulations. On the basis of our observations, it was tempting to suggest that the motions shown in the apo A2a AR simulations were those of the activation process while the motions in the A2a AR-ZMA simulations represented the inactive state. However, more caution needs to be exercised as it appears longer simulation time scales are required to verify this and a study by Dror et al.[94] had suggested the low likelihood of the former.

CONCLUSIONS

The behavior and conformational dynamics of the apo and liganded A2a adenosine receptors in MD simulations have been explored and analyzed in a detailed, quantitative, and unbiased way using PCA. The two main outcomes of this study are: (1) the convergence of protein dynamics for this system is not achievable in 200 ns, a time scale of the order of magnitude often used by current researchers in this and related fields; however, (2) by restricting ourselves to a very localized definition of convergence (intrahelical dynamics), we can fairly confidently conclude that interesting and variable dynamical behaviors are associated with the individual helices that are not directly predictable from crystal structure analysis. This study illustrates the power of replicate simulation strategies to identify the reliability of observations of dynamical behavior and of structurally sensitive techniques such as PCA to produce a more robust assessment of convergence and sampling than conventionally used parameters such as area per lipid, RMSDs, and energy terms. This said, it is unlikely that PCA-type analysis will directly correlate with an experimental observable, so it should be regarded as a surrogate, rather than direct, measure of adequate sampling or equilibration.

ASSOCIATED CONTENT

Supporting Information

Topology of ZM241385, porcupine plots, PC1/PC3 and PC3/PC2 plots, dot product matrices, RMSD plots, and table containing residues that constitute the 7-TM α-helices are provided. This material is available free of charge via the Internet at http://pubs.acs.org.

AUTHOR INFORMATION

Corresponding Author

*E-mail: Stephen.doughty@nottingham.edu.my. Phone: +603 89248200.

Author Contributions

S.W.D and C.A.L conceived the ideas in this work, and C.A.L provided expertise in PCA. H.W.N performed the computational work and simulations. H.W.N, C.A.L, and S.W.D contributed to the analysis. H.W.N and C.A.L prepared the manuscript.

Notes

The authors declare no competing financial interest.

ACKNOWLEDGMENTS

H.W.N. is grateful for the support from the University of Nottingham Malaysia Campus for the funding for this research.

ABBREVIATIONS

MD, molecular dynamics; GPCR, G-protein coupled receptors; AR, adenosine receptor; PCA, principal component analysis; EL, extracellular loop; IL, intracellular loop; POPC, palmitoyl-oleoyl-phosphatidylcholine; SPC, simple point charge; *NVT*, canonical ensemble; PME, smooth particle mesh Ewald; *NPT*, isothermal−isobaric ensemble; TM, transmembrane; PC, principal component; RMSD, root-mean-square deviation; RMSF, root-mean-square fluctuations

REFERENCES

(1) Klotz, L.; Boccon-Gibod, L.; Shore, N. D.; Andreou, C.; Persson, B. E.; Cantor, P.; Jensen, J. K.; Olesen, T. K.; Schroder, F. H. The efficacy and safety of degarelix: a 12-month, comparative, randomized, open-label, parallel-group phase III study in patients with prostate cancer. *BJU Int.* **2008**, *102*, 1531−1538.

(2) Abel, S.; Russell, D.; Whitlock, L. A.; Ridgway, C. E.; Nedderman, A. N.; Walker, D. K. Assessment of the absorption, metabolism and absolute bioavailability of maraviroc in healthy male subjects. *Br. J. Clin. Pharmacol.* **2008**, *65* (Suppl. 1), 60−67.

(3) Congreve, M.; Langmead, C. J.; Mason, J. S.; Marshall, F. H. Progress in structure based drug design for g protein-coupled receptors. *J. Med. Chem.* **2011**, *54*, 4283−4311.

(4) Tyndall, J. D.; Pfeiffer, B.; Abbenante, G.; Fairlie, D. P. Over one hundred peptide-activated G protein-coupled receptors recognize ligands with turn structure. *Chem. Rev.* **2005**, *105*, 793−826.

(5) Gruber, C. W.; Muttenthaler, M.; Freissmuth, M. Ligand-based peptide design and combinatorial peptide libraries to target G protein-coupled receptors. *Curr. Pharm. Des.* **2010**, *16*, 3071−3088.

(6) Nambi, P.; Aiyar, N. G protein-coupled receptors in drug discovery. *Assay Drug Dev. Technol.* **2003**, *1*, 305−310.

(7) Drews, J. Drug discovery: a historical perspective. *Science* **2000**, *287*, 1960−1964.
(8) Vassilatis, D. K.; Hohmann, J. G.; Zeng, H.; Li, F.; Ranchalis, J. E.; Mortrud, M. T.; Brown, A.; Rodriguez, S. S.; Weller, J. R.; Wright, A. C.; Bergmann, J. E.; Gaitanaris, G. A. The G protein-coupled receptor repertoires of human and mouse. *Proc. Natl. Acad. Sci. U.S.A.* **2003**, *100*, 4903−4908.
(9) Jacobson, K. A.; Gao, Z. G. Adenosine receptors as therapeutic targets. *Nat. Rev. Drug Discov.* **2006**, *5*, 247−264.
(10) Weiss, S. M.; Benwell, K.; Cliffe, I. A.; Gillespie, R. J.; Knight, A. R.; Lerpiniere, J.; Misra, A.; Pratt, R. M.; Revell, D.; Upton, R.; Dourish, C. T. Discovery of nonxanthine adenosine A2A receptor antagonists for the treatment of Parkinson's disease. *Neurology* **2003**, *61* (11 Suppl. 6), S101−106.
(11) Xu, K.; Bastia, E.; Schwarzschild, M. Therapeutic potential of adenosine A(2A) receptor antagonists in Parkinson's disease. *Pharmacol. Ther.* **2005**, *105*, 267−310.
(12) Hauser, R. A.; Schwarzschild, M. A. Adenosine A2A receptor antagonists for Parkinson's disease: rationale, therapeutic potential and clinical experience. *Drugs Aging* **2005**, *22*, 471−482.
(13) Dong, Q.; Ginsberg, H. N.; Erlanger, B. F. Overexpression of the A1 adenosine receptor in adipose tissue protects mice from obesity-related insulin resistance. *Diabetes Obes. Metab.* **2001**, *3*, 360−366.
(14) Baharav, E.; Bar-Yehuda, S.; Madi, L.; Silberman, D.; Rath-Wolfson, L.; Halpren, M.; Ochaion, A.; Weinberger, A.; Fishman, P. Antiinflammatory effect of A3 adenosine receptor agonists in murine autoimmune arthritis models. *J. Rheumatol.* **2005**, *32*, 469−476.
(15) Palczewski, K.; Kumasaka, T.; Hori, T.; Behnke, C. A.; Motoshima, H.; Fox, B. A.; Le Trong, I.; Teller, D. C.; Okada, T.; Stenkamp, R. E.; Yamamoto, M.; Miyano, M. Crystal structure of rhodopsin: A G protein-coupled receptor. *Science* **2000**, *289*, 739−745.
(16) Rasmussen, S. G.; Choi, H. J.; Rosenbaum, D. M.; Kobilka, T. S.; Thian, F. S.; Edwards, P. C.; Burghammer, M.; Ratnala, V. R.; Sanishvili, R.; Fischetti, R. F.; Schertler, G. F.; Weis, W. I.; Kobilka, B. K. Crystal structure of the human beta2 adrenergic G-protein-coupled receptor. *Nature* **2007**, *450*, 383−387.
(17) Warne, W.; Serrano-Vega, M. J.; Baker, J. G.; Moukhametzianov, R.; Edwards, P. C.; Henderson, R. Structure of a beta1-adrenergic G-protein-coupled receptor. *Nature* **2008**, *454*, 486−491.
(18) Jaakola, V. P.; Griffith, M. T.; Hanson, M. A.; Cherezov, V.; Chien, E. Y.; Lane, J. R.; Ijzerman, A. P.; Stevens, R. C. The 2.6 angstrom crystal structure of a human A2A adenosine receptor bound to an antagonist. *Science* **2008**, *322*, 1211−1217.
(19) Wu, B.; Chien, E. Y.; Mol, C. D.; Fenalti, G.; Liu, W.; Katritch, V.; Abagyan, R.; Brooun, A.; Wells, P.; Bi, F. C.; Hamel, D. J.; Kuhn, P.; Handel, T. M.; Cherezov, V.; Stevens, R. C. Structures of the CXCR4 chemokine GPCR with small-molecule and cyclic peptide antagonists. *Science* **2010**, *330*, 1066−1071.
(20) Chien, E. Y.; Liu, W.; Zhao, Q.; Katritch, V.; Han, G. W.; Hanson, M. A.; Shi, L.; Newman, A. H.; Javitch, J. A.; Cherezov, V.; Stevens, R. C. Structure of the human dopamine D3 receptor in complex with a D2/D3 selective antagonist. *Science* **2010**, *330*, 1091−5.
(21) Shimamura, T.; Shiroishi, M.; Weyand, S.; Tsujimoto, H.; Winter, G.; Katritch, V.; Abagyan, R.; Cherezov, V.; Liu, W.; Han, G. W.; Kobayashi, T.; Stevens, R. C.; Iwata, S. Structure of the human histamine H1 receptor complex with doxepin. *Nature* **2012**, *475*, 65−70.
(22) Haga, K.; Kruse, A. C.; Asada, H.; Yurugi-Kobayashi, T.; Shiroishi, M.; Zhang, C.; Weis, W. I.; Okada, T.; Kobilka, B. K.; Haga, T.; Kobayashi, T. Structure of the human M2 muscarinic acetylcholine receptor bound to an antagonist. *Nature* **2012**, *482*, 547−551.
(23) Kruse, A. C.; Hu, J.; Pan, A. C.; Arlow, D. H.; Rosenbaum, D. M.; Rosemond, E.; Green, H. F.; Liu, T.; Chae, P. S.; Dror, R. O.; Shaw, D. E.; Weis, W. I.; Wess, J.; Kobilka, B. K. Structure and dynamics of the M3 muscarinic acetylcholine receptor. *Nature* **2012**, *482*, 552−556.
(24) Hanson, M. A.; Roth, C. B.; Jo, E.; Griffith, M. T.; Scott, F. L.; Reinhart, G.; Desale, H.; Clemons, B.; Cahalan, S. M.; Schuerer, S. C.; Sanna, M. G.; Han, G. W.; Kuhn, P.; Rosen, H.; Stevens, R. C. Crystal structure of a lipid G protein-coupled receptor. *Science* **2012**, *335*, 851−855.
(25) Manglik, A.; Kruse, A. C.; Kobilka, T. S.; Thian, F. S.; Mathiesen, J. M.; Sunahara, R. K.; Pardo, L.; Weis, W. I.; Kobilka, B. K.; Granier, S. Crystal structure of the micro-opioid receptor bound to a morphinan antagonist. *Nature* **2012**, *485*, 321−326.
(26) Wu, H.; Wacker, D.; Mileni, M.; Katritch, V.; Han, G. W.; Vardy, E.; Liu, W.; Thompson, A. A.; Huang, X. P.; Carroll, F. I.; Mascarella, S. W.; Westkaemper, R. B.; Mosier, P. D.; Roth, B. L.; Cherezov, V.; Stevens, R. C. Structure of the human kappa-opioid receptor in complex with JDTic. *Nature* **2012**, *485*, 327−332.
(27) Granier, S.; Manglik, A.; Kruse, A. C.; Kobilka, T. S.; Thian, F. S.; Weis, W. I.; Kobilka, B. K. Structure of the delta-opioid receptor bound to naltrindole. *Nature* **2012**, *485*, 400−404.
(28) Thompson, A. A.; Liu, W.; Chun, E.; Katritch, V.; Wu, H.; Vardy, E.; Huang, X. P.; Trapella, C.; Guerrini, R.; Calo, G.; Roth, B. L.; Cherezov, V.; Stevens, R. C. Structure of the nociceptin/orphanin FQ receptor in complex with a peptide mimetic. *Nature* **2012**, *485*, 395−399.
(29) Park, S. H.; Das, B. B.; Casagrande, F.; Tian, Y.; Nothnagel, H. J.; Chu, M.; Kiefer, H.; Maier, K.; De Angelis, A. A.; Marassi, F. M.; Opella, S. J. Structure of the chemokine receptor CXCR1 in phospholipid bilayers. *Nature* **2012**, *491*, 779−783.
(30) White, J. F.; Noinaj, N.; Shibata, Y.; Love, J.; Kloss, B.; Xu, F.; Gvozdenovic-Jeremic, J.; Shah, P.; Shiloach, J.; Tate, C. G.; Grisshammer, R. Structure of the agonist-bound neurotensin receptor. *Nature* **2012**, *490*, 508−513.
(31) Zhang, C.; Srinivasan, Y.; Arlow, D. H.; Fung, J. J.; Palmer, D.; Zheng, Y.; Green, H. F.; Pandey, A.; Dror, R. O.; Shaw, D. E.; Weis, W. I.; Coughlin, S. R.; Kobilka, B. K. High-resolution crystal structure of human protease-activated receptor 1. *Nature* **2012**, *492*, 387−392.
(32) Rodriguez, D.; Pineiro, A.; Gutierrez-de-Teran, H. Molecular Dynamics Simulations Reveal Insights into Key Structural Elements of Adenosine Receptors. *Biochemistry* **2011**, *50*, 4194−4208.
(33) Filizola, M.; Wang, S. X.; Weinstein, H. Dynamic models of G-protein coupled receptor dimers: indications of asymmetry in the rhodopsin dimer from molecular dynamics simulations in a POPC bilayer. *J. Comput. Aided Mol. Des.* **2006**, *20*, 405−16.
(34) Rohrig, U. F.; Guidoni, L.; Rothlisberger, U. Early steps of the intramolecular signal transduction in rhodopsin explored by molecular dynamics simulations. *Biochemistry* **2002**, *41*, 10799−809.
(35) Ivanov, A. A.; Baskin, I. I.; Palyulin, V. A.; Piccagli, L.; Baraldi, P. G.; Zefirov, N. S. Molecular modeling and molecular dynamics simulation of the human A2B adenosine receptor. The study of the possible binding modes of the A2B receptor antagonists. *J. Med. Chem.* **2005**, *48*, 6813−6820.
(36) Arinaminpathy, Y.; Sansom, M. S.; Biggin, P. C. Molecular dynamics simulations of the ligand-binding domain of the ionotropic glutamate receptor GluR2. *Biophys. J.* **2002**, *82*, 676−683.
(37) Kaye, S. L.; Sansom, M. S.; Biggin, P. C. Molecular dynamics simulations of the ligand-binding domain of an N-methyl-D-aspartate receptor. *J. Biol. Chem.* **2006**, *281*, 12736−12742.
(38) Hallmen, C.; Wiese, M. Molecular dynamics simulation of the human adenosine A3 receptor: agonist induced conformational changes of Trp243. *J. Comput. Aided Mol. Des.* **2006**, *20*, 673−684.
(39) Crozier, P. S.; Stevens, M. J.; Forrest, L. R.; Woolf, T. B. Molecular dynamics simulation of dark-adapted rhodopsin in an explicit membrane bilayer: coupling between local retinal and larger scale conformational change. *J. Mol. Biol.* **2003**, *333*, 493−514.
(40) Chen, J. Z.; Wang, J.; Xie, X. Q. GPCR structure-based virtual screening approach for CB2 antagonist search. *J. Chem. Inf. Model.* **2007**, *47*, 1626−1637.
(41) Schlegel, B.; Laggner, C.; Meier, R.; Langer, T.; Schnell, D.; Seifert, R.; Stark, H.; Holtje, H. D.; Sippl, W. Generation of a homology model of the human histamine H(3) receptor for ligand

docking and pharmacophore-based screening. *J. Comput. Aided Mol. Des.* **2007**, *21*, 437−453.
(42) Yarnitzky, T.; Levit, A.; Niv, M. Y. Homology modeling of G-protein-coupled receptors with X-ray structures on the rise. *Curr. Opin. Drug Discov. Dev.* **2010**, *13*, 317−325.
(43) Obiol-Pardo, C.; Lopez, L.; Pastor, M.; Selent, J. Progress in the structural prediction of G protein-coupled receptors: D3 receptor in complex with eticlopride. *Proteins* **2011**, *79*, 1695−1703.
(44) Amadei, A.; Linssen, A. B.; Berendsen, H. J. Essential dynamics of proteins. *Proteins* **1993**, *17*, 412−425.
(45) Clarage, J. B.; Romo, T.; Andrews, B. K.; Pettitt, B. M.; Phillips, G. N., Jr. A sampling problem in molecular dynamics simulations of macromolecules. *Proc. Natl. Acad. Sci. U.S.A.* **1995**, *92*, 3288−3292.
(46) Balsera, M. W., W.; Oono, Y.; Shculten, K. Principal Component Analysis and Long Time Protein Dynamics. *J. Phys. Chem.* **1996**, *100*, 2567−2572.
(47) Amadei, A.; Ceruso, M. A.; Di Nola, A. On the convergence of the conformational coordinates basis set obtained by the essential dynamics analysis of proteins' molecular dynamics simulations. *Proteins* **1999**, *36*, 419−424.
(48) Hess, B. Similarities between principal components of protein dynamics and random diffusion. *Phys. Rev. E Stat. Phys. Plasmas Fluids Relat. Interdiscip. Topics* **2000**, *62*, 8438−8448.
(49) Hess, B. Convergence of sampling in protein simulations. *Phys. Rev. E Stat. Nonlin. Soft Matter. Phys* **2002**, *65*, 031910−031920.
(50) Faraldo-Gomez, J. D.; Forrest, L. R.; Baaden, M.; Bond, P. J.; Domene, C.; Patargias, G.; Cuthbertson, J.; Sansom, M. S. Conformational sampling and dynamics of membrane proteins from 10-ns computer simulations. *Proteins* **2004**, *57*, 783−791.
(51) Grossfield, A. S.; Feller, S. E.; Pitman, M. C. Convergence of Molecular Dynamics Simulations of Membrane Proteins. *Proteins* **2007**, *67*, 31−40.
(52) Romo, T. G. A. Block Covariance Overlap Method and Convergence in Molecular Dynamics Simulation. *J. Chem. Theory Comput.* **2011**, *7*, 2464−2472.
(53) Romo, T. D.; Grossfield, A. Validating and improving elastic network models with molecular dynamics simulations. *Proteins* **2011**, *79*, 23−34.
(54) *SYBYL Biopolymer modelling manual*, version 6.5; Tripos Inc.: St. Louis, MO, 1998; http://www.tripos.com.
(55) Oostenbrink, C.; Villa, A.; Mark, A. E.; van Gunsteren, W. F. A biomolecular force field based on the free enthalpy of hydration and solvation: The GROMOS force-field parameter sets 53A5 and 53A6. *J. Comput. Chem.* **2004**, *25*, 1656−1676.
(56) Berendsen, H. J. C.; van der Spoel, D. van drunen, R. GROMACS: A message-passing parallel molecular dynamics implementation. *Comput. Phys. Commun.* **1995**, *91*, 43−56.
(57) van der Spoel, D.; Lindahl, E.; Hess, B.; Groenhof, G.; Mark, A. E.; Berendsen, H. J. C. GROMACS: Fast, flexible, and free. *J. Comput. Chem.* **2005**, *26*, 1701−1718.
(58) Hess, B.; Kutzner, C.; van der spoel, D.; Lindahl, E. GROMACS 4: Algorithms for Highly Efficient, Load-Balanced, and Scalable Molecular Simulation. *J. Chem. Theory Comput.* **2008**, *4*, 435−447.
(59) Laskowski, R. A.; MacArthur, M. W.; Moss, D. S.; Thornton, J. M. PROCHECK: A program to check the stereochemical quality of protein structures. *J. Appl. Crystallogr.* **1993**, *26*, 283−291.
(60) Vriend, G. WHAT IF: A molecular modeling and drug design program. *J. Mol. Graph.* **1990**, *8*, 52−56.
(61) Schuttelkopf, A. W.; van Aalten, D. M. PRODRG: a tool for high-throughput crystallography of protein-ligand complexes. *Acta Crystallogr. D Biol. Crystallogr.* **2004**, *60*, 1355−1363.
(62) Lemkul, J. A.; Allen, W. J.; Bevan, D. R. Practical considerations for building GROMOS-compatible small-molecule topologies. *J. Chem. Inf. Model.* **2010**, *50*, 2221−2235.
(63) Berger, O.; Edholm, O.; Jahnig, F. Molecular dynamics simulations of a fluid bilayer of dipalmitoylphosphatidylcholine at full hydration, constant pressure, and constant temperature. *Biophys. J.* **1997**, *72*, 2002−2013.
(64) Wolf, M. G.; Hoefling, M.; Aponte-Santamaria, C.; Grubmuller, H.; Groenhof, G. g_membed: Efficient insertion of a membrane protein into an equilibrated lipid bilayer with minimal perturbation. *J. Comput. Chem.* **2010**, *31*, 2169−2174.
(65) Berendsen, H. J. C.; Postma, J. P. M.; van Gunsteren, W. F.; Hermans, J. Interaction Models for Water in Relation to Protein Hydration. In *In Intermolecular Forces*; Pullman, B., Ed.; Reidel Publishing Company: Reidel, Dordrecht, The Netherlands, 1981; pp 331−342.
(66) Essmann, U.; Perera, L.; Berkowitz, M. L. A smooth particle mesh Ewald method. *J. Chem. Phys.* **1995**, *103*, 8577−8593.
(67) Hess, B.; Bekker, H.; Berendsen, H. J. C.; Fraaije, J. G. E. M. LINCS: A Linear Constraint Solver for Molecular Simulations. *J. Comput. Chem.* **1997**, *18*, 1463−1472.
(68) Bussi, G.; Donadio, D.; Parinello, M. Canonical sampling through velocity rescaling. *J. Chem. Phys.* **2007**, *126*, 014101−014108.
(69) Parinello, M.; Rahman, A. Polymorphic transitions in single crystals: A new molecular dynamics method. *J. Appl. Phys.* **1981**, *52*, 7182−7190.
(70) Williams, T.; Kelley, C. *Gnuplot 4.5: an interactive plotting program*; 2011.
(71) Wallace, A. C.; Laskowski, R. A.; Thornton, J. M. LIGPLOT: a program to generate schematic diagrams of protein-ligand interactions. *Protein Eng.* **1995**, *8*, 127−134.
(72) Haider, S.; Parkinson, G. N.; Neidle, S. Molecular dynamics and principal components analysis of human telomeric quadruplex multimers. *Biophys. J.* **2008**, *95*, 296−311.
(73) Humphrey, W.; Dalke, A.; Schulten, K. VMD - Visual Molecular Dynamics. *J. Mol. Graph.* **1996**, *14*, 33−38.
(74) Rasmussen, S. G.; Choi, H. J.; Fung, J. J.; Pardon, E.; Casarosa, P.; Chae, P. S.; Devree, B. T.; Rosenbaum, D. M.; Thian, F. S.; Kobilka, T. S.; Schnapp, A.; Konetzki, I.; Sunahara, R. K.; Gellman, S. H.; Pautsch, A.; Steyaert, J.; Weis, W. I.; Kobilka, B. K. Structure of a nanobody-stabilized active state of the beta(2) adrenoceptor. *Nature* **2011**, *469*, 175−180.
(75) Wacker, D.; Fenalti, G.; Brown, M. A.; Katritch, V.; Abagyan, R.; Cherezov, V.; Stevens, R. C. Conserved binding mode of human beta2 adrenergic receptor inverse agonists and antagonist revealed by X-ray crystallography. *J. Am. Chem. Soc.* **2010**, *132*, 11443−11445.
(76) Li, J.; Edwards, P. C.; Burghammer, M.; Villa, C.; Schertler, G. F. Structure of bovine rhodopsin in a trigonal crystal form. *J. Mol. Biol.* **2004**, *343*, 1409−1438.
(77) Park, J. H.; Scheerer, P.; Hofmann, K. P.; Choe, H. W.; Ernst, O. P. Crystal structure of the ligand-free G-protein-coupled receptor opsin. *Nature* **2008**, *454*, 183−187.
(78) Xu, F.; Wu, H.; Katritch, V.; Han, G. W.; Jacobson, K. A.; Gao, Z. G.; Cherezov, V.; Stevens, R. C. Structure of an Agonist-Bound Human A2a Adenosine Receptor. *Science* **2011**, *332*, 322−327.
(79) Lebon, G.; Warne, T.; Edwards, P. C.; Bennett, K.; Langmead, C. J.; Leslie, A. G.; Tate, C. G. Agonist-bound adenosine A2A receptor structures reveal common features of GPCR activation. *Nature* **2011**, *474*, 521−525.
(80) Lyman, E.; Zuckerman, D. M. On the structural convergence of biomolecular simulations by determination of the effective sample size. *J. Phys. Chem. B* **2007**, *111*, 12876−12882.
(81) Grossfield, A.; Zuckerman, D. M. Quantifying uncertainty and sampling quality in biomolecular simulations. *Annu. Rep. Comput. Chem.* **2009**, *5*, 23−48.
(82) Myburgh, D. B.; Millar, R. P.; Hapgood, J. P. Alanine-261 in intracellular loop III of the human gonadotropin-releasing hormone receptor is crucial for G-protein coupling and receptor internalization. *Biochem. J.* **1998**, *331* (Pt 3), 893−896.
(83) Schulz, A.; Schoneberg, T.; Paschke, R.; Schultz, G.; Gudermann, T. Role of the third intracellular loop for the activation of gonadotropin receptors. *Mol. Endocrinol.* **1999**, *13*, 181−190.
(84) Angelova, K.; Fanelli, F.; Puett, D. Contributions of intracellular loops 2 and 3 of the lutropin receptor in Gs coupling. *Mol. Endocrinol.* **2008**, *22*, 126−38.

(85) Deupi, X.; Li, X. D.; Schertler, G. F. Ligands stabilize specific GPCR conformations: but how? *Structure* **2012**, *20*, 1289−1290.
(86) Dore, A. S.; Robertson, N.; Errey, J. C.; Ng, I.; Hollenstein, K.; Tehan, B.; Hurrell, E.; Bennett, K.; Congreve, M.; Magnani, F.; Tate, C. G.; Weir, M.; Marshall, F. H. Structure of the adenosine A(2A) receptor in complex with ZM241385 and the xanthines XAC and caffeine. *Structure* **2012**, *19*, 1283−1293.
(87) Liu, W.; Chun, E.; Thompson, A. A.; Chubukov, P.; Xu, F.; Katritch, V.; Han, G. W.; Roth, C. B.; Heitman, L. H.; AP, I. J.; Cherezov, V.; Stevens, R. C. Structural basis for allosteric regulation of GPCRs by sodium ions. *Science* **2012**, *337*, 232−236.
(88) Hino, T.; Arakawa, T.; Iwanari, H.; Yurugi-Kobayashi, T.; Ikeda-Suno, C.; Nakada-Nakura, Y.; Kusano-Arai, O.; Weyand, S.; Shimamura, T.; Nomura, N.; Cameron, A. D.; Kobayashi, T.; Hamakubo, T.; Iwata, S.; Murata, T. G-protein-coupled receptor inactivation by an allosteric inverse-agonist antibody. *Nature* **2012**, *482*, 237−240.
(89) Congreve, M.; Andrews, S. P.; Dore, A. S.; Hollenstein, K.; Hurrell, E.; Langmead, C. J.; Mason, J. S.; Ng, I. W.; Tehan, B.; Zhukov, A.; Weir, M.; Marshall, F. H. Discovery of 1,2,4-triazine derivatives as adenosine A(2A) antagonists using structure based drug design. *J. Med. Chem.* **2012**, *55*, 1898−1903.
(90) Ballesteros, J. A.; Jensen, A. D.; Liapakis, G.; Rasmussen, S. G.; Shi, L.; Gether, U.; Javitch, J. A. Activation of the beta 2-adrenergic receptor involves disruption of an ionic lock between the cytoplasmic ends of transmembrane segments 3 and 6. *J. Biol. Chem.* **2001**, *276*, 29171−29177.
(91) Shi, L.; Liapakis, G.; Xu, R.; Guarnieri, F.; Ballesteros, J. A.; Javitch, J. A. Beta2 adrenergic receptor activation. Modulation of the proline kink in transmembrane 6 by a rotamer toggle switch. *J. Biol. Chem.* **2002**, *277*, 40989−40996.
(92) Konopka, J. B.; Margarit, S. M.; Dube, P. Mutation of Pro-258 in transmembrane domain 6 constitutively activates the G protein-coupled alpha-factor receptor. *Proc. Natl. Acad. Sci. U.S.A.* **1996**, *93*, 6764−6769.
(93) Kim, S.-K.; Riley, L.; Abrol, R.; Jacobson, K. A.; Goddard, W. A. Predicted structures of agonist and antagonist bound complexes of adenosine A3 receptor. *Proteins* **2011**, *79*, 1878−1897.
(94) Dror, R. O.; Arlow, D. H.; Maragakis, P.; Mildorf, T. J.; Pan, A. C.; Xu, H.; Borhani, D. W.; Shaw, D. E. Activation mechanism of the beta2-adrenergic receptor. *Proc. Natl. Acad. Sci. U.S.A.* **2011**, *108*, 18684−18689.